Dissipative many-electron dynamics of ionizing systems

Jean Christophe Tremblay,[a] Stefan Klinkusch, Tillmann Klamroth, and Peter Saalfrank
Institut für Chemie, Universität Potsdam, Karl-Liebknecht-Straße 24-25, D-14476 Potsdam-Golm, Germany

(Received 1 October 2010; accepted 7 December 2010; published online 28 January 2011)

In this paper, we perform many-electron dynamics using the time-dependent configuration-interaction method in its reduced density matrix formulation (ρ-TDCI). Dissipation is treated implicitly using the Lindblad formalism. To include the effect of ionization on the state-resolved dynamics, we extend a recently introduced heuristic model for ionizing states to the ρ-TDCI method, which leads to a reduced density matrix evolution that is not norm-preserving. We apply the new method to the laser-driven excitation of H_2 in a strongly dissipative environment, for which the state-resolve lifetimes are tuned to a few femtoseconds, typical for dynamics of adsorbate at metallic surfaces. Further testing is made on the laser-induced intramolecular charge transfer in a quinone derivative as a model for a molecular switch. A modified scheme to treat ionizing states is proposed to reduce the computational burden associated with the density matrix propagation, and it is thoroughly tested and compared to the results obtained with the former model. The new approach scales favorably ($\sim N^2$) with the number of configurations N used to represent the reduced density matrix in the ρ-TDCI method, as compared to a N^3 scaling for the model in its original form. © *2011 American Institute of Physics*. [doi:10.1063/1.3532410]

I. INTRODUCTION

Many-electron dynamics continues to attract great interest from both theoreticians and experimentalists. Recent advances in experimental laser science have made it possible to create pulses shorter than a single cycle duration.[1–6] This allows to probe the dynamics of electrons on its natural time scale. Although great progress has been made in the description of many-electron systems in recent years,[7–36] the theory still lags behind the experiment for the time-dependent characterization of electronic properties of large molecules. There is thus a need to improve on the computational schemes available.

Among the different approaches to treat many-electron dynamics, wave function based methods such as time-dependent Hartree–Fock[7] and multiconfiguration time-dependent Hartree–Fock[18,23,37] appear very promising. Our method of choice is the time-dependent configuration-interaction (TDCI)[16] in which the electronic wave function is represented as a time-dependent linear combination of electronic configurations calculated at a chosen configuration-interaction (CI) level (CI singles, CI doubles, etc.). In principle, the methods converge toward the exact solution if the wave function expansion is large enough. Unfortunately, the problem becomes rapidly intractable and only relatively small systems can be treated exactly. A way around this limitation is to divide the full system in a subsystem including all important coordinates, and a bath including the remaining part of coordinate space. This type of separation is particularly natural when it comes to molecules adsorbed at surfaces or in electron-rich environments. The latter will be the focus of the present paper.

For so-called open systems, a reduced density matrix variant of the TDCI method was recently introduced.[38] As for the parent method, the reduced density matrix is represented in a basis of zeroth-order electronic states calculated using the CI methodology. Energy and phase relaxation are treated using the Lindblad formalism,[39] for which upward and downward projectors are used to represent dipole coupling through a chosen medium. A Kossakowski-like model is used to include the effect of pure dephasing of the zeroth-order states.[39–44] The main limitation of this method and TDCI in general is that the configurations associated with energies above the ionization threshold are strictly not bound since an electron can be lost to the environment. A heuristic model was introduced previously to include the effects of these so-called ionizing states on the dynamics in the TDCI method. It is one purpose of this communication to extend these ideas to the ρ-TDCI method.[34] To this effect, our main challenge will be the development of an efficient numerical scheme to render the evolution of the reduced density matrix tractable without compromising the quantitative description of the continuum.

II. MODELS AND METHODS

In this paper, we treat the dissipative many-electron dynamics of a molecule using the TDCI method[16] in its reduced density matrix form (ρ-TDCI).[38] First, the field-free electron Hamiltonian $\hat{H}_{\rm el}$ for an N_e electron system with N_a nuclei is written in the fixed nuclei approximation. The operator is represented in an appropriate set of electronic configurations, and the eigenvalues ϵ_n and the eigenvectors $|n\rangle$ of the resulting matrix are extracted using standard CI methodology at a desired level. The CI eigenvectors are then used to represent the reduced density matrix operator

$$\hat{\rho}(t) = \sum_{nm} \rho_{nm}(t)|n\rangle\langle m|, \tag{1}$$

[a]Electronic mail: jean.c.tremblay@gmail.com.

 © 2011 American Institute of Physics

Downloaded 15 Apr 2011 to 141.89.199.236. Redistribution subject to AIP license or copyright; see http://jcp.aip.org/about/rights_and_permissions

where $\rho_{nm}t$ are expansion coefficients. The evolution of the reduced density operator obeys the Liouville von Neumann equation (here in atomic units),

$$\frac{\partial\hat{\rho}(t)}{\partial t} = -i[\hat{H}_{\rm el}, \hat{\rho}(t)] + i[\underline{\hat{\mu}}\cdot\underline{F}(t), \hat{\rho}] + \mathcal{L}_D\hat{\rho}(t). \quad (2)$$

Here, the interaction between the system dipole $\hat{\mu}$ and an electric field $F(t)$ is treated in the semiclassical dipole approximation, and the dissipation of energy and phase through the contact with an environment is represented by the dissipative Liouvillian $\mathcal{L}_D$. To ensure semipositivity of the reduced density matrix, and thus a probabilistic interpretation of its diagonal element as population of the CI eigenstates, we chose to represent dissipation using the Lindblad semigroup formalism[39]

$$\mathcal{L}_D\hat{\rho}(t) = -\frac{1}{2}\sum_k([\hat{C}_k\hat{\rho}(t), \hat{C}_k^\dagger] + [\hat{C}_k, \hat{\rho}(t)\hat{C}_k^\dagger]). \quad (3)$$

The Lindblad operator $\hat{C}_k$ represents the kth dissipation channel. To treat energy dissipation upward and downward projectors are used,[38,42]

$$\hat{C}_k \to \sqrt{\Gamma_{m\to n}}|n\rangle\langle m|, \quad (4)$$

where $\Gamma_{m\to n}$ is the associated dissipation rate, chosen as in our previous work as a scaled Einstein coefficient for spontaneous emission,

$$\Gamma_{m\to n} = \frac{4A|\mu_{mn}|^2}{3c^3}\omega_{mn}^3, \quad (5)$$

where $\omega_{mn} = \epsilon_m - \epsilon_n$, $\mu_{mn} = \langle m|\hat{\mu}|n\rangle$, c is the speed of light, and A is a scaling factor to model electron-rich environments. Equation (5) holds for $m > n$, otherwise $\Gamma_{m\to n} = 0$ at $T = 0$ K. The most severe limitation of the ρ-TDCI method is the fixed nuclei approximation. For short time dynamics, molecular vibrations will lead to pure dephasing, which can be implicitly included by using a Kossakowski-like model[40,41]

$$\hat{C}_k \to \sqrt{\gamma^*}\hat{H}_{\rm el}, \quad (6)$$

where γ^* is a phenomenological pure dephasing rate. Note that in the formalism so far, the ρ-TDCI method is generally not energy-conserving, but norm-conserving, i.e., $\mathrm{Tr}[\hat{\rho}] = 1$. For a more detailed description of the ρ-TDCI method, the reader is referred to our previous work.[38,45]

In a typical CI calculation, most of the excited electronic states are found above the ionization potential (IP). The latter can be evaluated, e.g., using Koopmans' theorem and is depicted in Fig. 1 along with several electronic energy levels. The dipole coupling μ and the dissipation γ are also shown.

The m states below IP are bound, whereas the $N-m$ states above are strongly coupled with the continuum. That is, the electrons are unbound, as represented by the dotted arrow, and they should be considered to have a finite lifetime in the state above IP. This leads to the ionization of the molecule, for which the CI-states do not represent a good description of the electron density. In a previous paper,[34] a phenomenological model for including the lifetime of ionizing states has been introduced. The idea can be reformulated for the density matrix by adding a term to the Hamiltonian,

$$\hat{H}_{\rm el} \longrightarrow \hat{H}_{\rm el} - i\hat{W}, \quad (7)$$

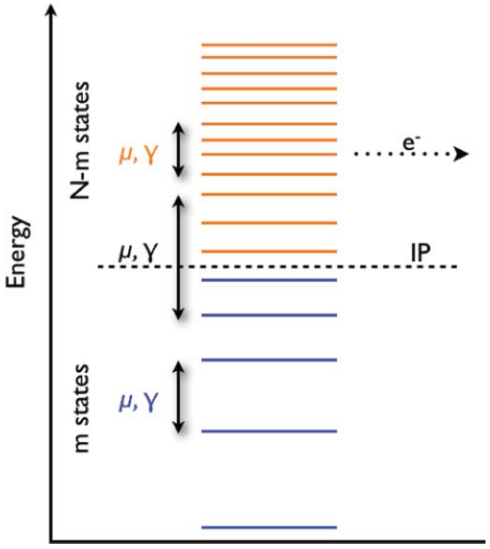

FIG. 1. Cartoon of the ionization process in a configuration-interaction basis of N electronic eigenstates. The m bound states located below the ionization potential (IP) are depicted in blue (dark gray). The $N-m$ ionizing states are depicted in orange (gray). The dipole moments μ and the dissipative rates γ are represented on the left in blue, orange, and black for the coupling among bound states, among ionizing states, and between the two groups, respectively.

where the "absorption" operator $\hat{W}$ is simply a sum of projectors on the CI states

$$\hat{W} = \sum_k \frac{I_k}{2}|k\rangle\langle k|. \quad (8)$$

Here, I_k is the ionization rate for a particular state k, which is a measure of its coupling to the continuum. Equations (7) and (8) imply that the reduced density matrix norm is lost as ionization proceeds. Alternatively, the norm could be preserved by using Lindblad operators $\hat{C}_k \to \sqrt{I_k}|v\rangle\langle k|$ which irreversibly transfer population from state $|k\rangle$ to an auxiliary "vacuum state" $|v\rangle$. The nature of this auxiliary state being unknown, we prefer to adopt the description of the continuum introduced above.

To evaluate the ionization rate, we consider that the energy $\mathcal{E}_r$ of an orbital above the ionization threshold will be completely transformed to kinetic energy of a single outgoing electron,

$$\mathcal{E}_r = v^2/2, \quad (9)$$

with velocity $v = d/\tau$. The escape length d is a free parameter that allows to scale the rates and τ can be interpreted as the lifetime of the orbital. The nth CI singles (CIS) wave function associated with energy $\epsilon_n^{\rm CIS}$is represented as a combination of the ground state Slater determinant $\Psi_0^{\rm HF}$ and selected excited configuration state functions ${}^1\Psi_a^r$,

$$|n\rangle = D_{0,n}\Psi_0^{\rm HF} + \sum_{a=L}^{N_e/2}\sum_{r=N_e/2+1}^{M} D_{a,n}^r\,{}^1\Psi_a^r. \quad (10)$$

Here, L is the index of the lowest occupied orbital that is not frozen and M that of the highest unfrozen unoccupied orbital. These excited configurations are obtained by bringing a single electron from an occupied orbital a to an unoccupied orbital r, both computed at the restricted Hartree–Fock level. Thus,

Downloaded 15 Apr 2011 to 141.89.199.236. Redistribution subject to AIP license or copyright; see http://jcp.aip.org/about/rights_and_permissions

the ionization rate of state n in this single electron picture can be defined as

$$I_n = \begin{cases} 0 & \text{if} \epsilon_{\mathrm{n}}^{\mathrm{CIS}} < IP \\ \sum_{a,r} |D_{a,n}^{r}|^2 \frac{\sqrt{2\mathcal{E}_r}}{d} & \text{if} \epsilon_{\mathrm{n}}^{\mathrm{CIS}} \geq IP \text{ and } \mathcal{E}_{\mathrm{r}} > 0 \end{cases}. \quad (11)$$

After transforming the operators in the interaction picture, e.g., $\hat{\rho}^{\mathcal{I}}(t) = e^{-i\hat{H}_{\mathrm{el}}t}\hat{\rho}(t)e^{i\hat{H}_{\mathrm{el}}t}$, the Liouville von Neumann equation with the modified Hamiltonian can be written in a basis of N configuration-interaction eigenvectors as

$$\frac{\mathrm{d}\rho_{mn}^{\mathcal{I}}}{\mathrm{d}t} = -e^{-i\omega_{mn}t}\left\{\left(\frac{I_m + I_n}{2}\right)\rho_{mn} - iF(t)\sum_{i=1}^{N}(\mu_{mi}\rho_{in} - \rho_{mi}\mu_{in}) + \gamma^*\omega_{mn}^2\rho_{mn} + \sum_{i=1}^{N}(\Gamma_{i\to n}\rho_{ii} - \Gamma_{n\to i}\rho_{nn})\delta_{mn} + \frac{1}{2}\sum_{i=1}^{N}(\Gamma_{m\to i} - \Gamma_{n\to i})\rho_{mn}\right\} e^{i\omega_{mn}t}. \quad (12)$$

These equations of motions can be integrated using a Runge–Kutta integrator, as already proved very efficient.[38,46,47] It can be seen that, to propagate the N^2 elements of the reduced density matrix, three summations over N elements are necessary. Thus, the propagation method scales effectively as N^3, which can become prohibitively expensive for large molecules. To circumvent this problem, an approximation can be made based on the numerical observation that coherence decay between ionizing states is very fast. This is affected by two main competing factors: dephasing and ionization. In our model, dephasing times are much longer than the ionization times and the reduced density matrix off-diagonal elements will vanish before the former affects the dynamics. Further, the CI configurations above IP are not physically correct: they are merely localized descriptions of states that couple strongly with the continuum. Since the states above IP are short-lived and their main purpose is to mediate the ionization process, it appears natural to neglect all dipole and dissipative couplings among them (represented in orange in Fig. 1). It is nonetheless important to keep the couplings between the states below and above IP, represented in black in Fig. 1, as they are responsible for the indirect coupling of the stable states to the continuum. The structure of the resulting rectangular matrix is shown in Fig. 2.

Only the diagonal elements of the density matrix and the gray blocks of size $m \times m$ and $(N-m) \times m$ are kept in memory and propagated. Because the number of states above IP $(N-m)$ is usually much larger than that of the states below IP (m), this results in immense memory and CPU time savings, as can be seen from inspection of Eq. (12). It will be shown in Sec. III that this approximation does not affect adversely the ultrafast laser-driven state-resolved electron dynamics for systems where ionization is faster than pure dephasing. In the following, the propagation including all coupling elements will be called "model 1" and the reduced model will be called "model 2."

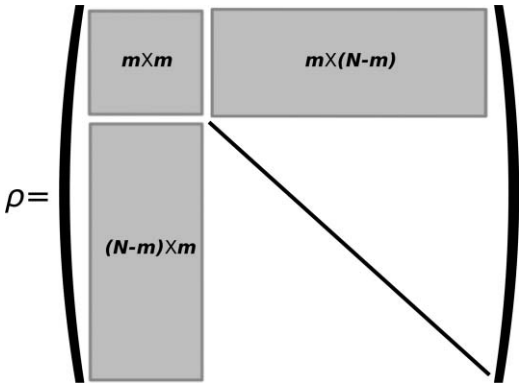

FIG. 2. Structure of the reduced density matrix for model 2. The couplings between the $(N-m)$ states above IP are neglected altogether. The associated coherences are kept to zero during the whole propagation. Only the $m \times m$ and $(N-m) \times m$ gray blocks, as well as diagonal elements of the $(N-m) \times (N-m)$ block are kept in memory and propagated.

III. NUMERICAL SIMULATIONS

A. Selective excitation of H2

To test the method on a toy problem, we applied model 1 to the selective excitation of molecular hydrogen up to the highest excited singlet state below the ionization barrier. The energy levels are obtained at the CIS(D) level of theory using Dunning's aug-cc-pVQZ basis.[48] The calculations are detailed elsewhere.[25,45] The first few states of the molecule are shown in Fig. 3. They are separated in levels that are accessible from the ground state using x-polarized, z-polarized, and y-polarized lasers (from left to right, respectively), with the molecular axis oriented along z. The ionization potential IP at 0.5945 E_h is denoted by the horizontal dashed line.

Only z-polarized excitations were performed here, where the target state $|5\rangle$ was reached either directly using a π-pulse or by sequentially pumping the population using a series of π-pulses of duration t_p,

$$F_z(t) = \sum_{k=1}^{n_p} F_{kz}U_k(t)\cos(\omega_k(t - t_p))$$
$$U_k(t) = \begin{cases} \sin^2\left(\frac{\pi(t-t_k)}{t_p}\right) & \text{for } t_k < t < t_k + t_p \\ 0 & \text{otherwise.} \end{cases} \quad (13)$$

The amplitude of the kth pulse, $F_{kz} = \frac{2\pi\hbar}{t_p|\mu_k|}$, is given as a function of the transition dipole moment μ_k for the given transition. The transition rates for the energy relaxation mechanism were calculated using Eq. (5) and scaled so that the lifetimes are in the femtosecond regime (e.g., $1/\Gamma_{1\to 0} = 45$ fs), which is typical for molecules adsorbed at metallic surfaces.[49] The scaling for the pure dephasing was chosen so that the dephasing rate between state $|0\rangle$ and $|1\rangle$ is the same

Downloaded 15 Apr 2011 to 141.89.199.236. Redistribution subject to AIP license or copyright; see http://jcp.aip.org/about/rights_and_permissions

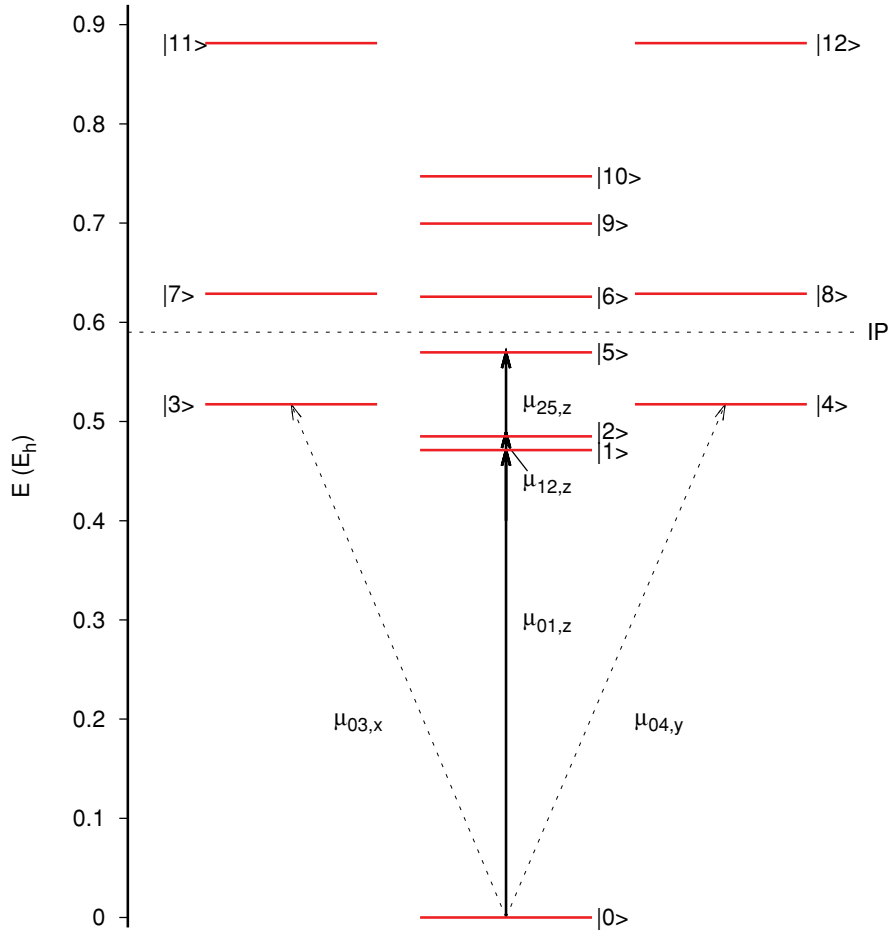

FIG. 3. Schematic representation of the first few eigenstates of the H_2 molecule computed at the CIS(D) level of theory using Dunning's aug-cc-pVQZ basis. The ionization barrier is at 0.5945 E_h. The energy levels are sorted according to the laser polarization with which they are accessible from the ground state. The degenerate $\{x, y\}$-states are depicted on the left and right, respectively. The z-polarized states are in the middle. The arrows represent the desired reaction pathway in three successive steps.

as its relaxation rate, $\gamma^* = \Gamma_{1\to 0}/\omega_{10}^2$. The escape length parameter was fixed at $d = 1.5$ Å to simulate very fast ionization processes.

Figure 4 shows the population dynamics for the direct excitation using a 24 fs π-pulse. The top left corner shows the evolution of the two relevant states, $|0\rangle$ and $|5\rangle$, for the free molecule without ionization. As expected, the population is quantitatively transferred to the target state by the π-pulse and the density matrix does not lose any norm (black solid line). The dynamics including dissipation also exhibit the expected pattern, as can be seen from the top right panel. The transfer yield is somewhat lower than for the free molecule and the population slowly goes back to the ground state at the end of the propagation.

Again, no norm is lost during the laser excitation. In the bottom left panel, the effect of ionization on the dynamics of the free molecule can be seen. Although the selectivity of the transition is preserved, excitation of higher excited states located above the ionization barrier leads to a loss of about 15% of the density matrix norm. The yield is reduced by the same amount. In the bottom right panel, it can be seen that the effects of dissipation and of ionization are almost linearly additive. Indeed, about 15% is lost to the continuum during the excitation and the population in the excited state exhibit a similar behavior as in the dissipative, nonionizing case.

Figure 5 shows the population dynamics for the excitation of state $|5\rangle$ using a series of nonoverlapping π-pulses. For the free molecule (top left panel), the first two pulses transfer almost quantitatively the population from the ground to the first and from the first to the second excited state, respectively. The wiggles in the populations between 20 and 30 fs are due to the molecule oscillating with the field, which contains only one and a half cycle for a 24 fs pulse with carrier frequency $\omega_{12} = 0.0139 E_h$. The third pulse, for the excitation from state $|2\rangle$ to state $|5\rangle$, is much less selective and the major part of the population is transferred to state $|9\rangle$, which is located above the ionization threshold. The intensity of the pulses simply allows for multiphoton excitations, which populates the undesired state. From the top right panel, it can be seen that including dissipation does not improve the selectivity, but merely reduces the yield of each transition from the ground state and up. The different relaxation rates cause different population decay for the intermediate states, but everything eventually comes down to the ground state, which is the dominant species at the end of the pulse sequence. In both the dissipative and nondissipative case, the norm of the reduced density matrix is preserved.

Downloaded 15 Apr 2011 to 141.89.199.236. Redistribution subject to AIP license or copyright; see http://jcp.aip.org/about/rights_and_permissions

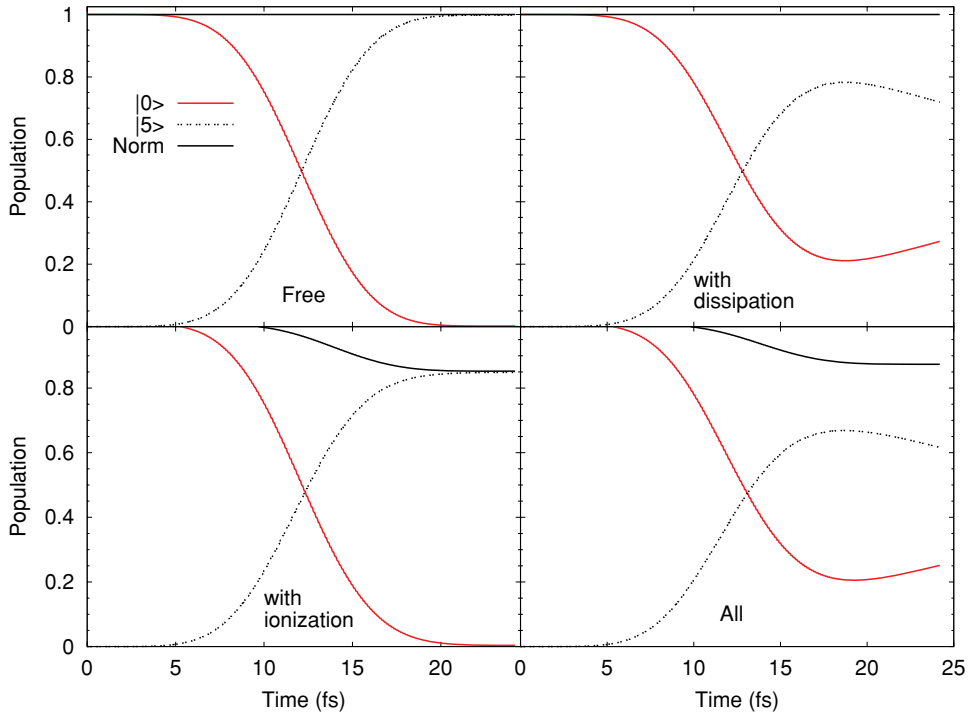

FIG. 4. Population evolution for the direct excitation of the highest electronic state below the ionization barrier for the rigid H_2 molecule, using a 24 fs π-pulse. Top left: free molecule in vacuum. Top right: molecule in dissipative environment. Bottom left: molecule in vacuum with ionization. Bottom right: molecule in dissipative environment with ionization.

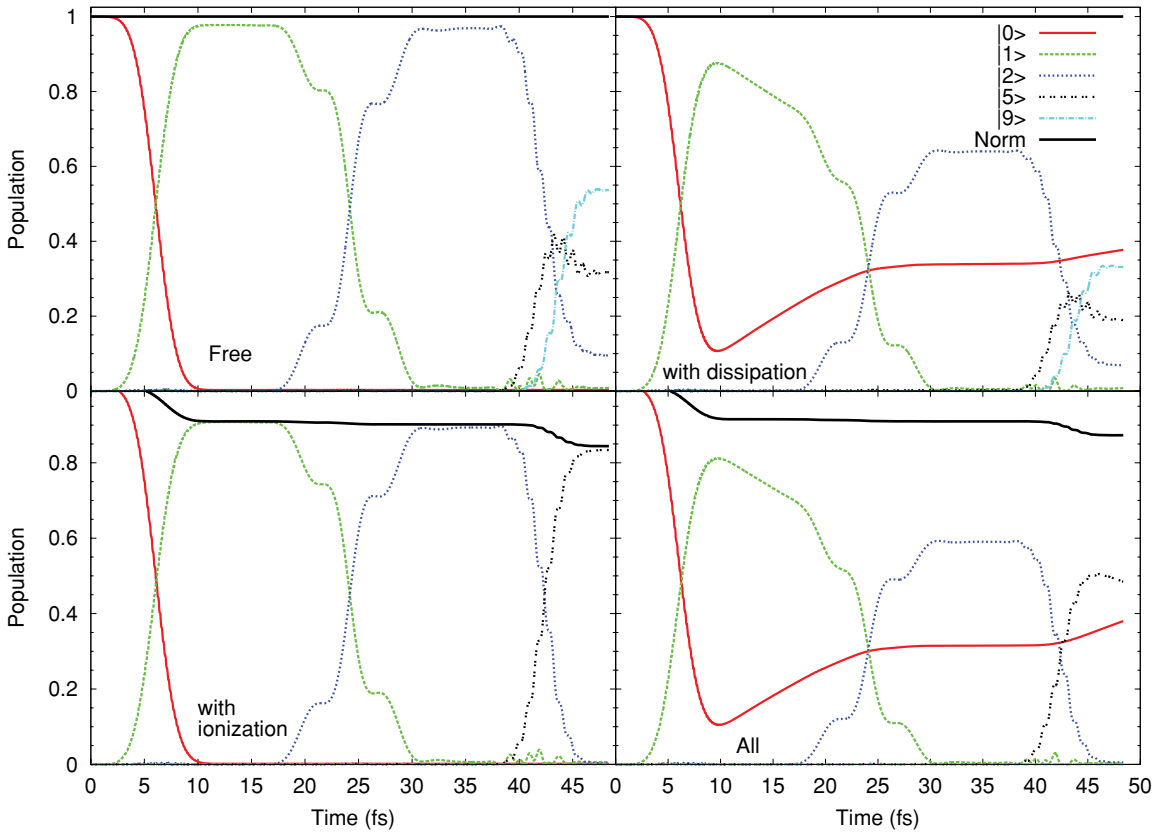

FIG. 5. Population evolution for the stepped excitation of the highest electronic state below the ionization barrier for the rigid H_2 molecule. A series of nonoverlapping π-pulses was used to pump the population coherently along the path $|0\rangle \rightarrow |1\rangle \rightarrow |2\rangle \rightarrow |5\rangle$. The pulse frequencies, durations, and amplitudes were chosen as $\{\omega_{01} = 0.4705E_h, F_{01} = 0.0127E_h/ea_0, t_p = 12\ \text{fs}\}$, $\{\omega_{12} = 0.0139E_h, F_{12} = 0.0022E_h/ea_0, t_p = 24\ \text{fs}\}$, and $\{\omega_{25} = 0.0839E_h, F_{25} = 0.0055E_h/ea_0, t_p = 12\ \text{fs}$, respectively. Top left: free molecule in vacuum. Top right: molecule in dissipative environment. Bottom left: molecule in vacuum with ionization. Bottom right: molecule in dissipative environment with ionization.

Downloaded 15 Apr 2011 to 141.89.199.236. Redistribution subject to AIP license or copyright; see http://jcp.aip.org/about/rights_and_permissions

By including ionization in our model, a drastic change in the selectivity can be seen for the last step of the excitation mechanism (see bottom panels). It appears that the undesirable state $|9\rangle$ is not at all populated and that the target state $|5\rangle$ is maximally populated. This observation is valid for both the free molecule and the molecule in a dissipative environment. In the latter case, the total yield is again affected adversely by dissipation, and population is found in both the ground and the target states at the end of the laser pulse sequence. The peculiar dynamical behavior can be rationalized by the fact that the laser-driven population transfer is mediated by the coherences, i.e., the off-diagonal elements of the density matrix. When ionization is included in the treatment, the coherences have a finite lifetime, which can be seen from the first term on the right-hand side of Eq. (12). Because of the very fast ionization rates, the coherences decay quickly and thus cannot mediate population transfer to higher excited states that would be otherwise accessible. In both panels in the bottom, the norm of the density matrix is reduced by about 15%, as for the direct excitation mechanism. The loss of norm appears to fluctuate depending on the state that is excited. For the first and the third transitions, about 10% and 5% of the norm is lost, whereas an almost negligible amount is lost at the second transition. This is simply explained by looking at the pulse intensities, with amplitudes as 0.012, 0.0021, and 0.0055 (all in atomic units) for the first, second, and third pulse, respectively. Hence, the larger the laser intensity is, the more population will be lost through ionization.

B. Intramolecular charge transfer

To study the properties of models 1 and 2, a much larger molecule, which shall provide a serious challenge for the ρ-TDCI method, is needed. We choose to study the selective excitation of the benzo[g]-*N*-methyl-quinolinium-7-hydroxylate (BMQ7H) molecule. The geometry of the molecule, optimized using GAUSSIAN 03[50] at the Restricted Hartree–Fock/6 − 31G* level of theory, is shown in Fig. 6.

The thin gray xy axes represent the standard orientation of the molecules in the ground state. The geometry of the fifth excited singlet state, which is the one targeted by our ultrafast laser excitation, has been overlaid on top of that of the ground state and the arrows show the displacement of each atom (in Angstrøm). The thick red axes define the convention for the dipole moment orientation, the z-axis coming out of the plane.

The optimized geometry was used for CIS calculation with a 6 − 31G* basis set using GAMESS07.[51] The wave functions and all dependent properties, e.g., the energies and the transition dipole moments, were computed at that level of theory. The 16 lowest orbitals were kept frozen and 246 molecular orbitals were used in the CIS calculation, which resulted in 8074 eigenstates for BMQ7H. The first few CIS states up to 1 E_h can be seen from Fig. 7 along with the ionization potential IP = $0.2057 E_h$, calculated using Koopmans' theorem.

Note that, although only a few states are shown here, various basis sizes were considered here, the largest of which had a maximal energy of 3.36 E_h. Nonetheless, already at energies

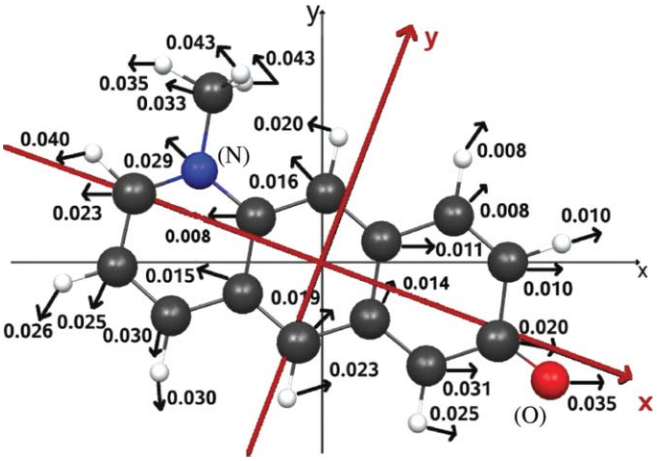

FIG. 6. Optimized structure of the BMQ7H molecule. The black, white, red, and blue balls represent carbon, hydrogen, oxygen (O), and nitrogen (N) atoms, respectively. The red (thick black) $\{x, y\}$-axes define the orientation of the dipole moment elements. The arrows define the displacement in the $\{x, y\}$ plane of the atoms in the fifth singlet excited state relative to the ground state. The magnitude of the displacements is given in Å.

about 1 E_h, the states are so dense that they appear as a quasicontinuum in the picture. Also depicted in the figure is the selected target state, $|5\rangle$, which can be readily excited from the ground state using an x-polarized laser pulse. The associated transition dipole moment is $\mu_{05,x} = -4.228\, ea_0$. A more detailed discussion of the molecule can be found elsewhere.[52]

The laser-induced state-resolved dissipative electron dynamics is shown in the top left panel of Fig. 8. A 5 fs π-pulse tuned at the $0 \rightarrow 5$ transition frequency was followed by a 20 fs decay to better show the effects of dissipation. In all dynamical simulations for BMQ7H, the lifetimes have been calculated using Eq. (5) and scaled so that the lifetimes are in the femtosecond regime (e.g., $1/\Gamma_{50} = 32$ fs). The pure dephasing constant has been set so that the pure dephasing

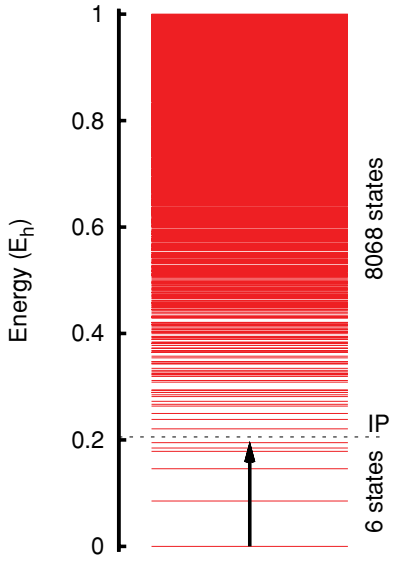

FIG. 7. Schematic representation of the low-lying electronic eigenstates of the BMQ7H molecule calculated at the CIS level of theory using a 6-31G* basis. The ionization barrier is at 0.2057 E_h. The excitation pathway for the intramolecular charge transfer is depicted by the thick black arrow.

Downloaded 15 Apr 2011 to 141.89.199.236. Redistribution subject to AIP license or copyright; see http://jcp.aip.org/about/rights_and_permissions

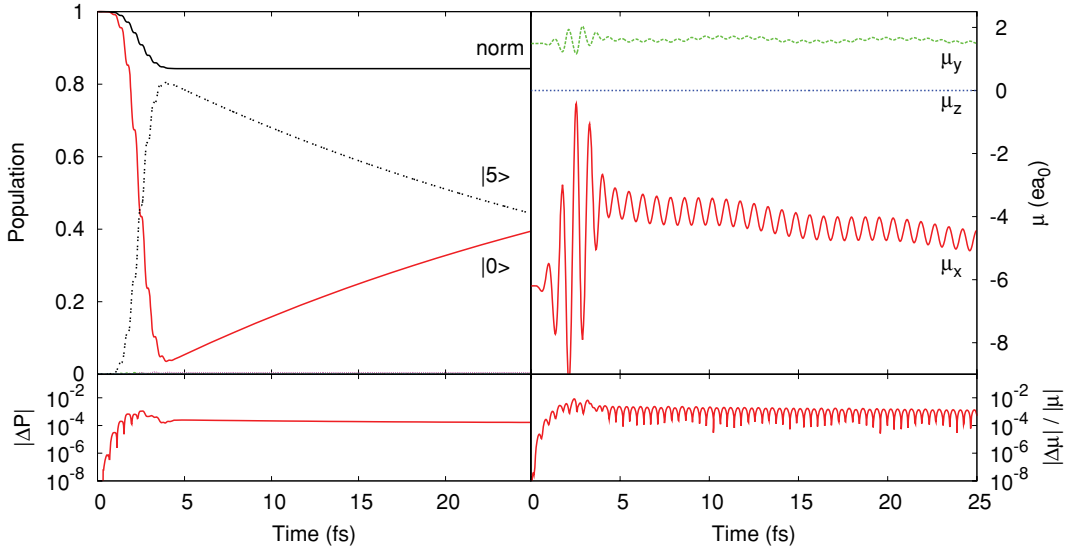

FIG. 8. Short-time dynamics for the intramolecular transfer in the BMQ7H molecule. The molecule is excited using a $\sin^2$ π-pulse of 5 fs duration ($\omega_{05} = 0.1949 E_h$, $F_{05} = 0.0071 E_h/ea_0$) followed by 20 fs of free decay. Top left: population evolution of the states below the ionization potential and of the reduced density matrix norm. Top right: evolution of the dipole moment components. Bottom left: difference between the populations from the two numerical schemes. Bottom right: relative difference between the dipole moment obtained with the two numerical schemes.

rate for the first transition is the same as the energy relaxation rate, $\gamma^* = \Gamma_{1\to 0}/\omega_{10}$. The escape length parameter was again set to $d = 1.5$ Å. The results shown use model 1 to include ionization and a basis of 1600 CIS eigenstates up to an energy of 1.265. As was the case for the direct excitation of the H_2 molecule, the population inversion is indeed affected by the presence of both ionization and dissipation. The former can be seen by the loss of norm during the excitation, meaning that a fraction of the population is lost to the continuum by ionization. The latter can be seen from the fact that the π-pulse does not transfer the population to the desired state $|5\rangle$ and that some remains in the ground state. The selectivity of the transition is very high, but the remaining population in the ground state leads to the creation of a wave packet.

The oscillations of the wave packet can be seen from the top right panel of the figure, which depicts from top to bottom the expectation value of the dipole moment along the y, z, and x, respectively. After an initial period where the oscillations have large amplitude due to the interaction with the laser field, the expectation values oscillate with two dominant frequencies, which are better seen from the x and y components. During the free evolution, relaxation to the ground state causes a return of the dipole moment to its original value, as should be expected.

The bottom part of Fig. 8 shows a measure of the differences between the aforementioned quantities obtained with either model 1 or model 2. The square root of the sum of squares of population difference of all states, $|\Delta P|$, is shown in the bottom left panel, from which it can be seen that the maximum deviation between the two models is below 0.1% during the laser excitation. The difference remains about constant at $|\Delta P| \sim 0.01\%$ during the free decay since most ionization already took place by the end of the pulse. The exponential decay of the ionizing states cannot be seen on this scale. This level of discrepancy is about the same as the relative difference in the dipole moment, as seen from the bottom right panel. The wave packet that is created at the end of the pulse is slightly different for both models, which affects slightly the dynamics at longer time. That is, oscillations are seen in the relative dipole difference during the free decay period, which contrasts with the behavior of the population difference. Nonetheless, both models appear to yield quantitatively similar results.

The difference between the two models depends somewhat on the intensity of the laser used for the excitation. Figure 9 shows the evolution of the reduced density matrix norm as a function of the laser fluence, using 5 fs $\sin^2$ pulses and $N = 1600$ as above.

For very low field amplitudes ($F_0 = 5 \times 10^{-3} E_h/ea_0$, $F_0 = 10^{-2} E_h/ea_0$) the density matrix norm is numerically almost equal. As the laser fluence increases, the discrepancies between the two ionization models become larger and most of the population is lost through ionization. When using fields of ludicrous amplitude ($F_0 = 10^{-1} E_h/ea_0$, $F_0 = 5 \times 10^{-2} E_h/ea_0$), all the population is lost by the time the laser pulse reaches its maximum intensity. In these cases, the differences between models 1 and 2 are larger, but the dynamics using both models mirrors the other, with equal phase and asymptotic behavior. It can be argued that the two models are of equal quality, since the excited states above the ionization potential are merely there to mediate the coupling of an electron to the continuum. The quantitative difference seen at larger laser fluence can be attributed to the different approaches to describe these couplings.

When exciting an ionizing system in the femtosecond regime, many states above the ionization barrier will be populated. An ultrafast laser pulse will have a large energy width, which can lead to broadband excitation. Further, for large laser intensities the zeroth-order states will be strongly coupled and they cannot be strictly considered as true eigenstates

Downloaded 15 Apr 2011 to 141.89.199.236. Redistribution subject to AIP license or copyright; see http://jcp.aip.org/about/rights_and_permissions

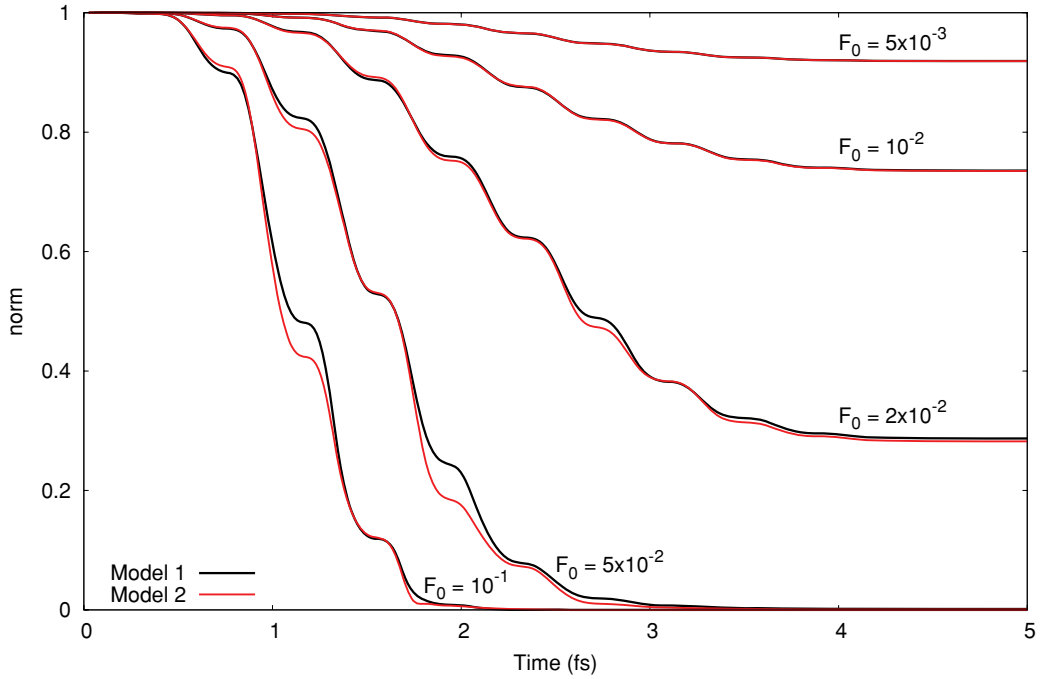

FIG. 9. Effect of the field amplitude on the reduced density matrix norm for 5 fs $\sin^2\pi$-pulses. The red (gray) and black curves are associated with the full and alternate numerical schemes, respectively. The field amplitude F_0 is given in units of E_h/ea_0.

of the system. The inclusion of many excited states is thus necessary to recover the correct electron dynamics during a short and intense pulse. This can be understood as using a basis of CI functions to represent the time coordinate. A key issue is thus to make sure that enough states above the ionization barrier are included in the basis to treat the coupling of the low-lying states to the continuum appropriately. The more states are included, the higher the coupling to the continuum and the higher loss of norm should be expected from the dynamics. Figure 10 shows the effect of increasing the basis size N on the loss of norm of the density matrix for both ionization models 1 and 2 (left and right panels, respectively). Only the excitation period using a 5 fs π-pulse to invert the population from the ground to the 5th excited state is shown, as only during this period, the reduced density matrix norm is affected by the ionization model.

For a given basis size, both evolution yields quantitatively similar behavior, as was shown previously for the state-resolved dynamics and the associated dipole expectation value. When using a very small basis of $N = 100$ CIS eigenstates, the loss of norm is clearly underestimated. As the basis size is increased to $N = 1600$, both models are almost converged. This is where model 1 reaches its limits because of the associated computational burden. On the other hand, it is still possible to increase the basis size for model 2 up to $N = 6400$. It is clear that a $N = 1600$ basis is not enough

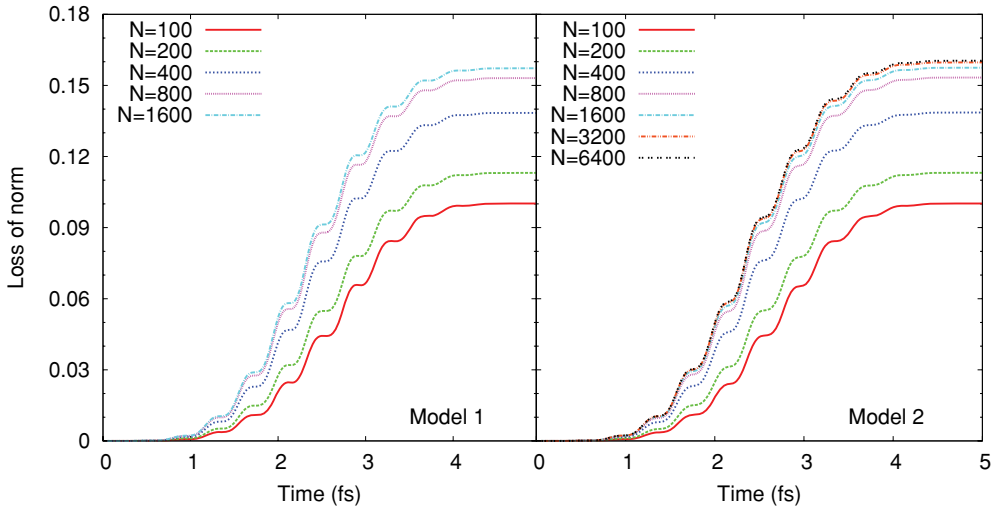

FIG. 10. Effect of the basis size on the convergence of the excitation dynamics. The loss of norm is depicted on the left for the first numerical model. In the right panel, the loss of norm is shown for the second, more efficient numerical model.

Downloaded 15 Apr 2011 to 141.89.199.236. Redistribution subject to AIP license or copyright; see http://jcp.aip.org/about/rights_and_permissions

to fully converge the dynamics, as the loss of norm still increases slightly when 3200 and 6400 CIS eigenstates are used to represent the reduced density matrix operator. It appears that the largest basis that can be used in model 1 is not big enough to yield converged dynamics. The small discrepancies between the two models (see Figs. 8 and 9) thus justify the use of model 2, which allows to include more basis functions and to better converge the dynamics.

A main advantage of model 2 over model 1 is thus that the computational burden associated with the former is much reduced as compared to that of the latter. The memory requirements for model 1 and model 2 both scale like N^2, but the latter is about a factor 4 smaller than the latter in our current implementation. This can amount to significant savings for larger basis sizes. The bottleneck of the ρ-TDCI method is the calculation time, as the propagation in the original form scales at best as N^3. The main advantage of model 2 resides in its CPU time scaling, which is about N times faster than model 1: the latter scales as $\sim N^3$, whereas the former scales as $\sim N^2$. This in appearance insignificant difference amounts to huge savings for large bases. For example, it takes about the same time for the simulation with model 2 using $N = 6400$ basis functions as for the simulation with model 1 using $N = 400$ configurations in the example presented here. Since the number states above the ionization barrier is expected to be much larger than that of the states below for most molecules (e.g., there are 6 bound states and 8068 ionizing states for BMQ7H), we expect this trend to be valid in general. A great feature of model 2 is thus to reduce the CPU time scaling of the ρ-TDCI method to the same scaling as that of the parent method for a simple electronic wave function propagation, the time-dependent configuration-interaction. This allows to converge the basis size without compromising the quality of the dynamical simulation.

IV. CONCLUSIONS

In conclusion, we have proposed an extension of the time-dependent configuration-interaction method in its reduced density matrix form to include the effects of ionization in the electron dynamics of a molecule in a dissipative environment. Energy and phase relaxation are included using Lindblad operators, for which the rates are scaled so that the lifetime are in the femtosecond regime to mimic the effect of an electron-rich medium on the dynamics. The ionization is included phenomenologically by introducing an imaginary projection operator, which leads to a not norm-preserving evolution of the reduced density matrix. This loss of norm accounts for the loss of an electron by the molecule via ionization. The ionization rates are computed in the single electron picture using a heuristic model based on the excess energy of orbitals located above the ionization threshold.

Application to a toy problem has shown that ionization indeed affects the selectivity and the yield of laser-driven ultrafast excitations. It appears that excluding ionization in the treatment of electron dynamics driven by short, intense laser pulses could lead to erroneous simulations. Further, it seems that dissipation and ionization have additive effects on the dynamics and that they do not affect each other directly. The selective excitation of an intramolecular charge transfer state in a prototypical molecule, benzo[g]-*N*-methyl-quinolinium-7-hydroxylate, has shown similar trends.

For the latter model problem, an alternate treatment of ionization was introduced which is valid for systems where ionization is faster than dephasing. The new model yields results that are in quantitative agreement with the phenomenological treatment presented above, but discrepancies arise when the intensity of the exciting laser field becomes very large. The main feature of the alternate scheme for ionization is its numerical efficiency. As compared to the full ionization treatment, the new model is less memory demanding but still scales as N^2 for a basis of N CI eigenvectors. The main savings come from the CPU time, which scales favorably as $\sim N^2$ for the system studied, as compared to $\sim N^3$ for the original model. This renders the alternate treatment better suited for the study of larger molecules, where the size of the CI basis can become prohibitively large. The basis size was shown to be an important parameter to converge the dynamics in the presence of dissipation and ionization. It is hoped that the new method will allow for an accurate and efficient simulation of larger systems, for example, semiconductor quantum dots embedded in semiconductor and metallic matrices.

ACKNOWLEDGMENTS

This work was supported by the Sonderforschungbereich 658, subproject C2 of the Deutsche Forschungsgemeinschaft.

[1] M. Hentschel, R. Kienberger, C. Spielmann, G. A. Reider, N. Milosevic, T. Brabek, P. Corkum, U. Heinzmann, M. Drescher, and F. Krausz, Nature (London) **414**, 509 (2001).
[2] R. Kienberger, M. Hentschel, M. Uibracker, C. Spielmann, M. Kitzler, A. Scrinzi, M. Wieland, T. Westerwalbesloh, U. Kleineberg, U. Heinzmann, M. Drescher, and F. Krausz, Science **297**, 1144 (2002).
[3] M. Drescher, R. Hentschel, M. Kienberger, M. Uibracker, V. Yakovlev, A. Scrinzi, T. Westerwalbesloh, U. Kleineberg, U. Heinzmann, and F. Krausz, Nature (London) **419**, 803 (2002).
[4] P. H. Bucksbaum, Nature (London) **421**, 593 (2003).
[5] G. G. Paulus, F. Lindner, H. Walther, A. Baltuka, E. Goulielmakis, M. Lezius, and F. Krausz, Phys. Rev. Lett. **91**, 253004 (2003).
[6] A. Föhlisch, P. Feulner, F. Hennies, D. Fink, A. Menzel, P. M. Sanchez-Portal, D. Echenique, and W. Wurth, Nature (London) **436**, 373 (2005).
[7] K. Kulander, Phys. Rev. A **36**, 2762 (1987).
[8] R. Grobe and J. H. Eberly, Phys. Rev. A **48**, 4664 (1993).
[9] M. Pindzola, P. Gavras, and T. Gorczyca, Phys. Rev. A **51**, 3999 (1995).
[10] H. Yu and A. Bandrauk, Phys. Rev. A **56**, 685 (1997).
[11] F. Remacle and R. Levine, J. Chem. Phys. **110**, 5089 (1999).
[12] F. Calvayrac, P.-G. Reinhard, E. Suraud, and C. Ullrich, Phys. Rep. **337**, 493 (2000).
[13] K. Harumiya, I. Kawata, H. Kono, and Y. Fujimura, J. Chem. Phys. **113**, 8953 (2000).
[14] J. Breidbach and L. Cederbaum, J. Chem. Phys. **118**, 3983 (2003).
[15] M. Suzuki and S. Mukamel, J. Chem. Phys. **119**, 4722 (2003).
[16] T. Klamroth, Phys. Rev. B **68**, 245421 (2003).
[17] S. Laulan and H. Bachau, Phys. Rev. A **68**, 013409 (2003).
[18] J. Zanghellini, M. Kitzler, C. Fabian, T. Brabec, and A. Scrinzi, Laser Phys. **13**, 1064 (2003).
[19] T. Kato and H. Kono, Chem. Phys. Lett. **392**, 533 (2004).
[20] X. Chu and S. I. Chu, Phys. Rev. A **70**, 61402 (2004).
[21] G. Paramonov, Chem. Phys. Lett. **411**, 305 (2005).
[22] T. Burnus, M. Marques, and E. Gross, Phys. Rev. A **71**, 010501 (2005).
[23] M. Nest, T. Klamroth, and P. Saalfrank, J. Chem. Phys. **122**, 124102 (2005).
[24] P. Krause, T. Klamroth, and P. Saalfrank, J. Chem. Phys. **123**, 074105 (2005).

Downloaded 15 Apr 2011 to 141.89.199.236. Redistribution subject to AIP license or copyright; see http://jcp.aip.org/about/rights_and_permissions

[25]P. Krause, T. Klamroth, and P. Saalfrank, J. Chem. Phys. **127**, 034107 (2007).
[26]I. Barth and J. Manz, Angew. Chem. Int. Ed. **45**, 2962 (2006).
[27]I. Barth, J. Manz, Y. Shigeta, and K. Yagi, J. Am. Chem. Soc. **128**, 7043 (2006).
[28]T. Klamroth, J. Chem. Phys. **124**, 144310 (2006).
[29]A. Castro, M. Marques, H. Appel, M. Oliveira, C. Rozzi, X. Andrade, F. Lorenzen, E. Gross, and A. Rubio, Phys. Status Solidi B **243**, 2465 (2006).
[30]H. Schlegel, S. Smith, and X. Li, J. Chem. Phys. **126**, 244110 (2007).
[31]B. Schäfer-Bung and M. Nest, Phys. Rev. A **78**, 012512 (2008).
[32]J. Schmidt, E. Goulielmakis, and V. S. Yakovlev, J. Phys. B: At. Mol. Opt. Phys. **41**, 115602 (2008).
[33]S. Klinkusch, T. Klamroth, and P. Saalfrank, Phys. Chem. Chem. Phys. **11**, 3875 (2009).
[34]S. Klinkusch, P. Saalfrank, and T. Klamroth, J. Chem. Phys. **131**, 114304 (2009).
[35]T. Klamroth and M. Nest, Phys. Chem. Chem. Phys. **11**, 349 (2009).
[36]M. Nest, Chem. Phys. Lett. **472**, 171 (2009).
[37]T. Kato and H. Kono, Chem. Phys. Lett. **392**, 533 (2004).
[38]J. C. Tremblay, T. Klamroth, and P. Saalfrank, J. Chem. Phys. **129**, 084302 (2008).
[39]G. Lindblad, Commun. Math. Phys. **48**, 119 (1976).
[40]V. Gorini, A. Kossakowski, and E. C.G. Sudarshan, J. Math. Phys. **17**, 821 (1976).
[41]V. Gorini and A. Kossakowski, J. Math. Phys. **17**, 1298 (1976).
[42]R. Kosloff, M. Ratner, and W. B. Davis, J. Chem. Phys. **106**, 7036 (1997).
[43]D. M. Lockwood, M. Ratner, and R. Kosloff, Chem. Phys. **268**, 55 (2001).
[44]E. A. Weiss, G. Katz, R. H. Goldsmith, M. R. Wasielewski, M. Ratner, R. Kosloff, and A. Nitzan, J. Chem. Phys. **124**, 074501 (2006).
[45]J. C. Tremblay, P. Krause, T. Klamroth, and P. Saalfrank, Phys. Rev. A **81**, 063420 (2010).
[46]J. C. Tremblay and T. Carrington, Jr., J. Chem. Phys. **121**, 11535 (2004).
[47]J. C. Tremblay and P. Saalfrank, Phys. Rev. A **78**, 063408 (2008).
[48]A. K. Wilson, T. van Mourik, and T. H. Dunning, J. Mol. Struct. **388**, 339 (1996).
[49]P. Saalfrank, Chem. Rev. **106**, 4116 (2006).
[50]M. J. Frisch, G. W. Trucks, H. B. Schlegel *et al.*, GAUSSIAN03, *Revision C.02*, Gaussian, Inc., Wallingford, CT, 2004.
[51]M. W. Schmidt, K. K. Baldridge, J. A. Boatz, S. T. Elbert, M. S. Gordon, J. J. Jensen, S. Koseki, N. Matsunaga, K. A. Nguyen, S. J. Su, T. L. Windus, M. Dupuis, and J. A. Montgomery, J. Comput. Chem. **13**, 1347 (1993).
[52]S. Klinkusch and T. Klamroth, "Simulations of pump-probe excitations of electronic wave packets for a large quasi-rigid molecular system by means of an extension of the time-dependent configuration-interaction singles method" (submitted).

Downloaded 15 Apr 2011 to 141.89.199.236. Redistribution subject to AIP license or copyright; see http://jcp.aip.org/about/rights_and_permissions